

## Structural chemistry of Mn, Fe, Co, and Ni in manganese hydrous oxides: Part II. Information from EXAFS spectroscopy and electron and X-ray diffraction

ALAIN MANCEAU\*

Laboratoire de Minéralogie-Cristallographie, Universités Paris 6 et 7, CNRS UA09, Tour 16, 4 place Jussieu,  
75252 Paris Cedex 05, France

ANATOLII I. GORSHKOV

Institute of Ore Geology and Mineralogy (IGEM) of the USSR Academy of Science, 35 Staromonetny prospekt,  
109017 Moscow, Russia

VICTOR A. DRITS

Geological Institute of the USSR Academy of Science, 7 Pyzhevsky prospekt, 109017 Moscow, Russia

### ABSTRACT

The short- and long-range structural order of various hydrous oxides were investigated using extended X-ray absorption fine structure (EXAFS), X-ray and electron diffraction (XRD and SAED) and in situ chemical analysis (EDS). Materials examined include synthetic sodium birnessite, natural magnesium birnessite, natural nickel copper birnessite, synthetic vernadite ( $\delta$ -MnO<sub>2</sub>), a series of natural iron vernadite samples, natural manganese goethite, two natural cobalt nickel asbolane samples, and natural cobalt asbolane. The structure of birnessite is similar to that of chalcophanite, but there are no corner-sharing Mn<sup>4+</sup>-Mn<sup>4+</sup> octahedra. Sodium and magnesium birnessite differ primarily in the stacking mode of their Mn octahedral sheets and their interlayer structure. Similarities and differences between these two minerals have been considered in terms of anion close-packed models. In contrast to birnessite, synthetic vernadite ( $\delta$ -MnO<sub>2</sub>) has edge- and corner-sharing Mn<sup>4+</sup> octahedra and a three-dimensional anionic framework;  $\delta$ -MnO<sub>2</sub> does not appear to be a *c*-disordered birnessite. In iron vernadite and manganese goethite, Fe<sup>3+</sup> and Mn<sup>4+</sup> ions are segregated in coherent scattering domains. In both minerals, Mn atoms form phylломanganate-like domains; in iron vernadite, Fe domains have a ferroxhite-like local structure. Asbolane has been found to have a mixed-layer structure. Cobalt nickel asbolane has layers of MnO<sub>2</sub>, Ni(OH)<sub>2</sub>, and possibly CoOOH or Co(OH)<sub>3</sub> alternating regularly along the *c* axis. In cobalt asbolane, Mn<sup>2+</sup> tetrahedral layers are presumably regularly interstratified with layers of MnO<sub>2</sub> and (CoOOH). This study provides new examples of hybrid structures among low-temperature materials and confirms their heterogeneous nature on a very fine scale.

### INTRODUCTION

Characterization of many hydrous manganese oxides by structural methods is difficult and frequently incomplete because of their poor crystallinity. Structural methods can be divided into two groups: the diffraction techniques are sensitive to medium- and long-range order, and the spectroscopic techniques are sensitive to electronic or local structure. Our present knowledge of hydrous manganese oxide structure is based mostly on the former. The tectomanganates have a relatively good crystallinity and have been well characterized. Significant studies of the past 15 years include Chukhrov et al. (1978a, 1979, 1981, 1985a, 1986), Turner and Buseck (1981), Post et al. (1982), Miura (1986), Vicat et al. (1986), and Post and Bish (1988). In contrast, most phylломanga-

nates have a lower degree of crystallinity, so few of their structures have been refined. Some studies of phylломanganates include birnessite and buserite: Giovanoli et al. (1970a, 1970b), Chukhrov et al. (1985b, 1987a), Strobel et al. (1987), and Post and Veblen (1990); vernadite: Chukhrov et al. (1988); asbolane: Chukhrov et al. (1980, 1987b), Drits (1987), Manceau et al. (1987); and mixed-layer buserite-asbolane: Chukhrov et al. (1983, 1987b).

The main difficulties in the study of poorly crystallized hydrous manganese oxides are that (1) their X-ray diffraction (XRD) patterns usually contain only a few broad, weak reflections, and (2) several minerals (buserite, asbolane, mixed-layer asbolane-buserite) give nearly the same XRD patterns (Drits et al., 1985). Recently, however, some progress has been made in simulating diffraction effects of defect structure models (Drits and Tchoubar, 1990; Chukhrov et al., 1989), and in applying the Rietveld method for structure refinement of some of the

\* Present address: Université Joseph Fourier, LGIT, BP 53X,  
38041 Grenoble Cedex, France.

better crystallized samples (Post and Veblen, 1990). Selected area electron diffraction (SAED) has also proven useful for the structural analysis of hydrous manganese oxides. Two characteristics that distinguish this method from XRD are its higher sensitivity to long-range order (Drits, 1987) and the possibility of focusing the electron beam on a small volume, thus allowing identification of discrete phases in a polymineral matrix. For instance, the combination of XRD and SAED completed with in situ chemical analysis (energy dispersive spectroscopy, EDS) has permitted the determination of the structure of metal-containing asbolanes and mixed-layer buserite-asbolanes. However, even at the micrometer scale, diffraction methods yield average structures at best. These are often not the same as actual structure for at least two reasons: (1) natural manganese oxides often contain large amounts of Fe, and the similarity in scattering power of Mn and Fe prevents their distinction by diffraction techniques; (2) minor and trace elements in manganese oxides cause local zones of different structure.

Several spectroscopic methods have been used to refine the structural chemistry of manganese oxides. Some of these, such as extended X-ray absorption fine structure (EXAFS) and infrared spectroscopy (IR), are sensitive to local or near-local structure (Potter and Rossman, 1979; Manceau et al., 1987; Manceau and Combes, 1988; Stouff and Boulègue, 1988; Manceau, 1989; Manceau et al., 1989, 1990a). The main advantages of X-ray absorption spectroscopy (XAS = EXAFS + XANES) are threefold: (1) almost all elements are spectroscopically active; (2) the structural information comes from more than the nearest coordination sphere of the X-ray absorber; and (3) the spectra from specific elements can usually be obtained separately. These aspects make XAS a valuable tool for determining a particular atom's local environment and for probing its electronic structure. The main limitation of XAS is its lack of spatial resolution in comparison to SAED; that limits XAS use to single phases, i.e., where the X-ray absorber phase is unique.

This paper extends the work begun in the XANES study of hydrous manganese oxides that was presented by Manceau et al. (1992). In this second part, we have combined data from EXAFS, XANES, XRD, SAED, and EDS. Our aims are (1) to clarify the structure of natural and synthetic birnessite, (2) to examine the possible structural relationship between vernadite and birnessite, (3) to determine the structural environments of Mn and Fe in natural iron vernadite and manganese goethite, and (4) to better define the structure of asbolanes.

## EXPERIMENTAL DETAILS

### Techniques

**EXAFS spectroscopy.** We used the EXAFS IV station at the LURE synchrotron radiation laboratory (Orsay, France). The positron energy of the storage ring DCI was 1.85 GeV, and the current was between 200 and 250 mA. The incident beam was monochromatized with pairs of

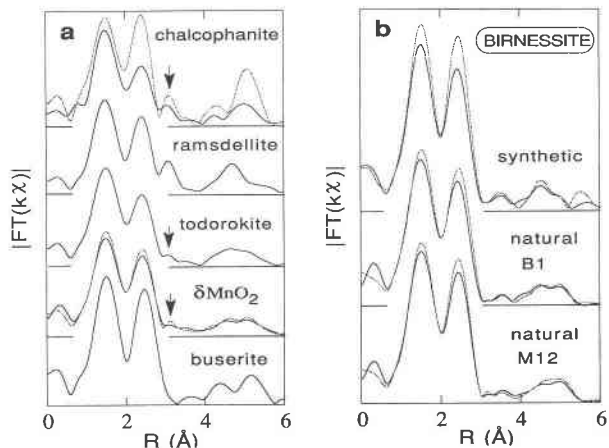


Fig. 1. MnK RDF of reference compounds,  $\delta$ -MnO<sub>2</sub> and birnessite. Solid line = room temperature (RT), dotted line = lower temperature. (a) From lowest upward: buserite (RT),  $\delta$ -MnO<sub>2</sub> (RT, 4.5 K), todorokite, ramsdellite, and chalcophanite (RT, 30 K). Notice the similarity of RDF of todorokite and  $\delta$ -MnO<sub>2</sub>. Arrow indicates MnO<sub>6</sub> corner-linked contributions. (b) From lowest upward: sample M12 (RT, 77 K), sample B1 (RT, 77 K), synthetic birnessite (Na<sub>2</sub>Mn<sub>14</sub>O<sub>27</sub>·9H<sub>2</sub>O) (RT, 4.5 K). RDF have not been corrected for phase shifts.

reflecting Si (311) crystals. Harmonics due to high order reflections were eliminated with borosilicate glass mirrors (Saintavit et al., 1988). EXAFS data were reduced using the plane-wave approximation with a standard procedure (Teo, 1986). To maximize the detection limit of atomic contributions (namely corner-sharing octahedra), (1) we obtained spectra at room temperature and at low temperature (77 K or 4.5 K) (Fig. 1a), and (2) we attempted to reduce spurious peaks in the MnK RDF (radial distribution function) caused by cutoff effects during the Fourier transform. These Fourier transform artifacts were minimized by using the Kaiser window with a  $\tau$  parameter of 3. In such conditions, the detection limit for corner-sharing Me atoms (Me = Mn, Zn . . .) is lower than one Me per Mn atom (Manceau and Combes, 1988).

**X-ray and electron diffraction and energy dispersive analysis.** XRD patterns of powdered samples were recorded with a DRON-UM or with a Siemens diffractometer using CuK $\alpha$  radiation and a graphite monochromator. SAED patterns and EDS spectra were obtained using a JEM-100C microscope equipped with a Kevex spectrometer with a voltage of 100 kV and a nominal current. Samples were dispersed in aqueous solution with an ultrasonic disperser. Thin colloid films covered with C were used as support, and grids were mounted on a tilting sample holder. Techniques for treating SAED patterns have been described by Drits (1987).

### Materials

**Reference minerals.** A series of well-crystallized manganese oxides (Manceau and Combes, 1988), and other Mn-, Fe-, and Co-bearing minerals were analyzed to serve

**TABLE 1.** Name and ideal composition of references and samples

Mineral	Ideal composition	Reference
<b>Manganese oxides</b>		
Phyllomanganates		
Buserite (2-D)	MnO <sub>2</sub>	1
Birnessite (2-D)	Na <sub>x</sub> Mn <sub>1-x</sub> O <sub>27</sub> ·9H <sub>2</sub> O	2
Asbolane (2-D)	Mn(O,OH) <sub>2/3</sub> (Ni,Co) <sub>x</sub> (O,OH) <sub>2</sub> ·nH <sub>2</sub> O	3
Chalcophanite (2-D')	ZnMn <sub>3</sub> O <sub>7</sub> ·3H <sub>2</sub> O	4
Vernadite (2-D')	δ-MnO <sub>2</sub>	5
Tectomanganates (3-D)		
Todorokite	(Na,Ca,K) <sub>0.3-0.7</sub> (Mn,Mg) <sub>6</sub> O <sub>12</sub> ·nH <sub>2</sub> O	6
Ramsdellite	α-MnO <sub>2</sub>	7
<b>Iron oxides</b>		
Goethite	α-FeOOH	8
Akaganeite	β-FeOOH	9
Lepidocrocite	γ-FeOOH	10
Feroxyhite	δ-FeOOH	11
Ferrihydrite	5Fe <sub>2</sub> O <sub>3</sub> ·9H <sub>2</sub> O	12
Hematite	α-Fe <sub>2</sub> O <sub>3</sub>	13
<b>Cobalt oxide</b>		
Heterogenite	CoOOH	14

Note: 1 = Giovanoli (1980b); 2 = Post and Veblen (1990); 3 = Drits (1987); 4 = Wadsley (1953), Post and Appleman (1988); 5 = Chukhrov et al. (1978b), Giovanoli (1980a); 6 = Post and Bish (1988); 7 = Byström (1949); 8 = Szytula et al. (1968); 9 = Szytula et al. (1970); 10 = Ewing (1935); 11 = Patrat et al. (1983); 12 = Towe and Bradley (1967); 13 = Blake et al. (1966); 14 = Delaplane et al. (1969), Deliens and Goethals (1973).

as reference compounds. The minerals are listed in Table 1 along with their ideal chemical formulae.

**Samples.** The minerals under study include synthetic sodium birnessite, two natural birnessite samples (sample B1 which contains some Mg, Ca, K, and Na, and sample M12, which contains some Ni and Cu), synthetic vernadite (δ-MnO<sub>2</sub>), a series of natural iron vernadite samples, natural manganese goethite, two natural cobalt nickel asbolanes (samples asb and Mn-ox), and natural cobalt asbolane. Details concerning the nature, origin, and chemical composition of the samples, as well as some selected crystallographic data, can be found in Manceau et al. (1992) (hereafter referred to as Part I). A summary of those data is given in Table 1.

## RESULTS

### Reference minerals

Figure 1a shows the MnK RDF obtained for several reference tetravalent manganates. The first three peaks in the spectra of chalcophanite, ramsdellite, and todorokite correspond to contributions from the nearest O atomic shell and from the nearest two Mn shells, respectively (Manceau and Combes, 1988). For all manganese oxides, the first Mn shell is located at approximately 2.90 Å and corresponds to MnO<sub>6</sub> octahedra linked by edges. This peak is always present because MnO<sub>2</sub> structures are built of single or multiple octahedral chains (Fig. 2; Part I). The second Mn shell at approximately 3.4–3.5 Å (arrow) is characteristic of minerals that have MnO<sub>6</sub> octahedra linked by corners. Of interest, here, is the correlation of this next-nearest cation contribution with the type of O framework. Two dimensional (2-D) layer structures (such as buserite and lithiophorite) have no corner-sharing octahedra while 2-D' structures (such as chalcophanite,

which has Zn atoms lying above and below vacant Mn octahedra), have a few (Fig. 2; Part I).

### Birnessite

The XRD pattern of our synthetic sample is quite similar to that of synthetic sodium birnessite studied by Post and Veblen (1990) (data not shown). The measured *d* values indicate a one-layer, monoclinic unit cell having parameters *a* = 5.174 Å, *b* = 2.848 Å, *c* = 7.336 Å, β = 103.2°. In contrast, our natural samples have a hexagonal unit cell with *a* = *b* = 2.84 Å, *c* = 7.10 Å, γ = 120°, similar to the results of Chukhrov et al. (1985b).

SAED patterns of synthetic birnessite particles show the same reflections as XRD patterns, but in addition they show a weak set of *hk0* super reflections as described by Giovanoli et al. (1970a), Chukhrov et al. (1989), and Post and Veblen (1990). Thus the unit-cell parameters determined from XRD do not correspond to the actual dimensional periodicity in the *ab* plane. Extra reflections indicating superperiodicity are missing on SAED patterns of natural birnessite particles.

The MnK RDF for the birnessite samples are plotted in Figure 1b; the curve for natural sample B1 is identical to that of the synthetic one. They show a single Mn peak corresponding to a Mn<sup>4+</sup> shell at 2.9 Å. The other natural birnessite sample (M12) shows a small second Me contribution (Me = Mn, Co, Ni, or Cu) at about 3.4–3.5 Å at both analysis temperatures.

### Vernadite

Diffraction features of vernadite (δ-MnO<sub>2</sub>) and of the iron vernadite samples have been reported by Chukhrov et al. (1987c, 1988). The XRD patterns are nearly identical; most show only two broad reflections, but some have an additional, weak, shoulderlike reflection at *d* ≈ 2.2 Å. We observed the same diffraction features in SAED patterns from most particles (Fig. 2a). However, a few particles have more Fe than Mn, and these display SAED patterns that have four ring reflections at 2.55, 2.24, 1.71, and 1.47 Å (compare Fig. 2a and 2b with Fig. 2c and 2d). The SAED patterns of these particles resemble that of feroxyhite (δ-FeOOH); hence we assume that their structure is similar to that of feroxyhite.

The MnK RDF for synthetic δ-MnO<sub>2</sub> resembles that of todorokite (Fig. 1a). A similarity in structural chemical features of these two minerals was also observed in the pre-edge and main-edge *K* XANES spectra reported in Part I. MnK RDF for natural vernadite (Fig. 3a) also resemble that of todorokite, even to the point of displaying a weak but significant (Mn,Fe) contribution at 3.4 Å.

The most striking result from the vernadite study is the close similarity of the FeK RDF for iron vernadite and feroxyhite (Fig. 3b). This likeness is confirmed by comparing their Fourier-filtered Fe-(Fe,Mn) contributions (Fig. 4a). The corresponding Fe-Fe contributions for goethite are considerable different in phase and amplitude. These vernadite spectra were best fitted by assuming two nearest Fe-Fe pairings at 2.89 and 3.03 Å, as in δ-FeOOH (Fig. 4b). Mn and Fe have similar backscattering ampli-

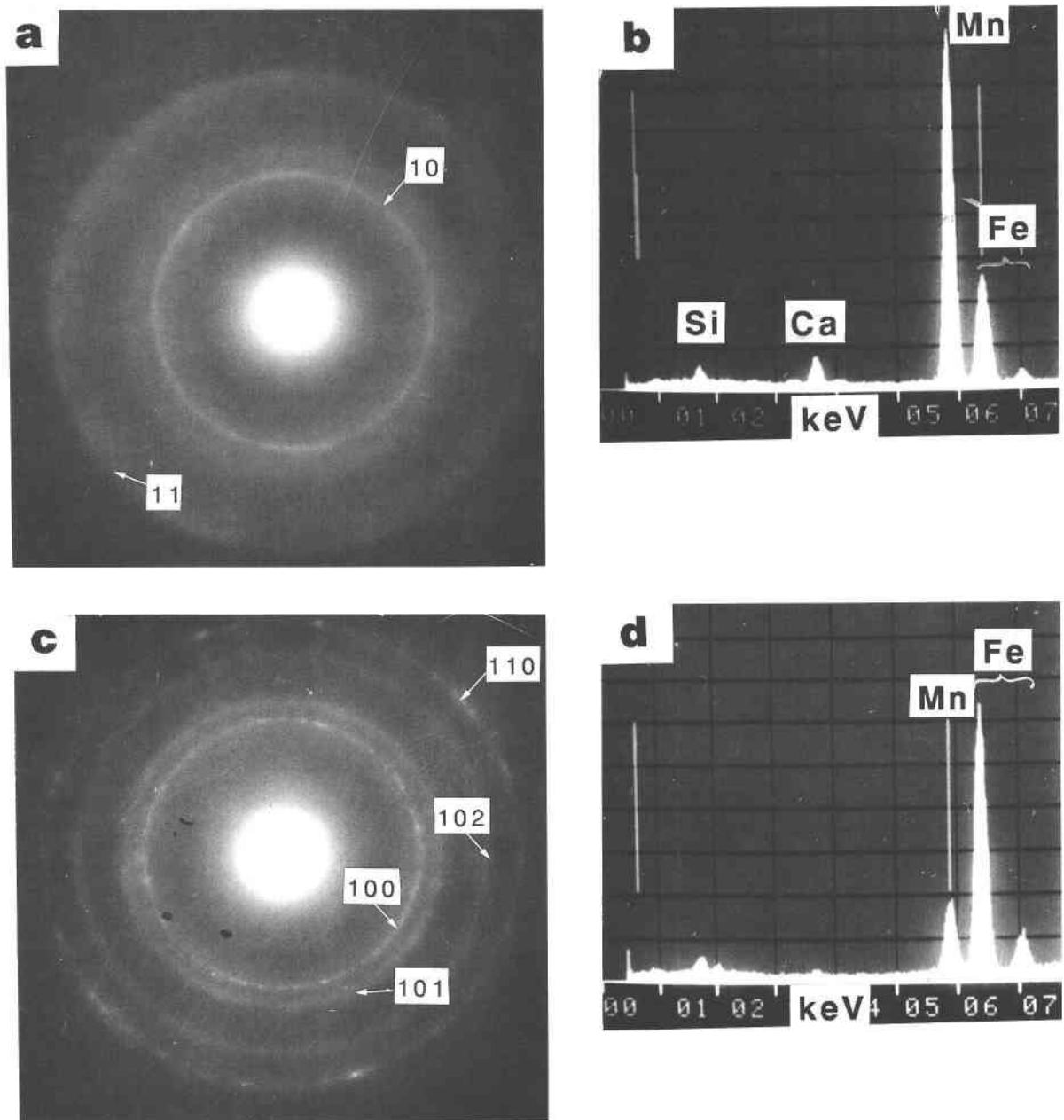


Fig. 2. SAED patterns and EDS spectra for Fe-bearing vernadite particles. (a), (b) Representative of most of the particles where there is a higher concentration of Mn than Fe. SAED patterns contain only two  $hk$  bands; (c), (d) particles where Fe is more abundant than Mn. SAED pattern resembles that of ferroxihite.

tudes and phase shifts functions, so EXAFS cannot differentiate between the two; thus, a good fit would also have been obtained by assuming Mn instead of Fe nearest neighbors. However, the presence of Fe in the vicinity of Fe is supported by the fact that Mn and Fe atoms possess a different local structure.

#### Mn-bearing goethite

The XRD pattern for manganese goethite shows broadened  $hkl$  reflections that have approximately the same  $d$  values as those of goethite (Fig. 5). No manganese oxide

impurity was detected; a lack of even trace quantities of groutite is proved by the absence of reflections near 2.81, 2.38, and 2.30 Å (see arrows). Figure 6a is a TEM image of some sample particles; EDS analyses show that they all contain similar amounts of Mn and Fe, although the concentration of Fe is usually slightly greater (Fig. 6c). In spite of a high Mn content, SAED patterns are characterized by the same reflections as those expected for goethite, which confirm the monomineralic nature of this manganese goethite at the scale sampled by diffraction techniques (Fig. 6b).

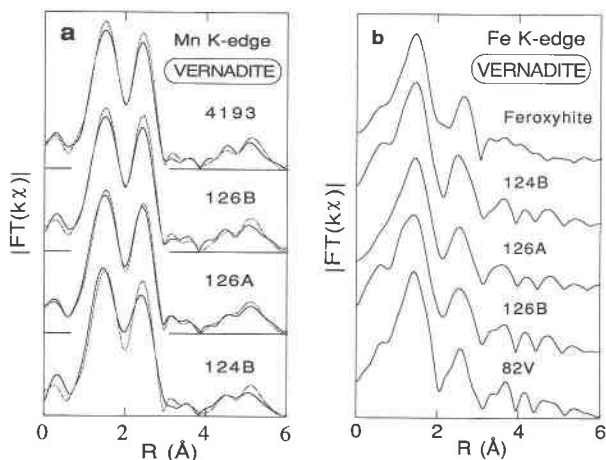


Fig. 3. EXAFS data for iron vernadite samples. (a) MnK RDF. Solid line = RT, dotted line = 77 K. Data were analyzed using a Kaiser window with  $\tau = 3.0$ . (b) Compare shape of FeK RDF to that of ferroxihite. Data were analyzed using Hanning + flat window (Manceau and Combes, 1988). RDF have not been corrected for phase shifts.

The FeK RDF for this sample (Fig. 7a) is identical to that of goethite (Manceau and Combes, 1988). The MnK RDF contains well-defined second and third peaks whose intensities are comparable to those of todorokite (Fig. 7). The similarity in the local Mn environment in goethite and in todorokite has been verified by Fourier-filtering Mn-O and Mn-Mn contributions. The Mn-(O,OH) distance is equal to 1.90–1.92 Å, a value consistent with a tetravalent state for Mn ions.

### Asbolane

Previous results showed that none of the asbolane samples were completely monomineralic (see description in Part I). Sample asb and the cobalt asbolane from Germany also contain small amounts of cobalt busserite and calcium busserite, respectively. Periodicity along the c axis for asbolane and busserite are not the same; they are 9.5 and 7 Å, respectively (under vacuum conditions). Sample Mn-ox contains lithiophorite as an impurity.

SAED patterns for most of the Co,Ni-bearing asbolane

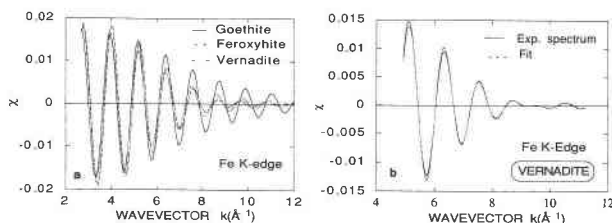


Fig. 4. Fourier-filtered nearest Fe-Fe contributions to EXAFS. (a) Experimental data for goethite, ferroxihite, and vernadite sample 126B. (b) Fit for vernadite sample 124B. Notice that the wave beating at about 9–10 Å<sup>-1</sup> is reproduced well by assuming two Fe shells at 2.89 and 3.03 Å, corresponding to face and edge linkage, respectively.

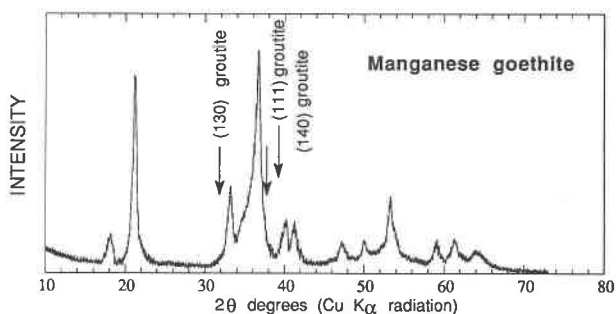


Fig. 5. XRD pattern for manganese goethite. No MnO<sub>2</sub> impurity is detected. Arrows correspond to the (130), (111), and (140) reflections of goethite.

particles of samples asb and Mn-ox contain two incommensurate hexagonal networks of  $hk0$  reflections and a unique series of basal  $00l$  reflections (Fig. 8). The structures of these particles can be described by two sublattices having different hexagonal unit-cell parameters in the  $ab$  plane ( $a_I = b_I = 2.84$  Å for sublattice I, and  $a_{II} = b_{II} = 3.01$  Å for sublattice II) but a common periodicity perpendicular to them along  $c$  ( $c = 9.40$  Å). Our SAED reflection intensity distributions are the same as those for the cobalt nickel asbolane and nickel asbolane particles described by Chukhrov et al. (1980). In each reciprocal sublattice the 100 reflection is about half as intense as that of 110 (Fig. 8), but for each given  $hk0$  reflection, reciprocal sublattice I reflections are stronger than reciprocal sublattice II reflections (e.g., compare  $11_I$  and  $11_{II}$  in Fig. 8a, 8c). EDS spectra show that Ni concentration varies in the particles of cobalt nickel asbolane. Our observations show that with smaller Ni content, the  $hk0$  reflection intensities for sublattice II are weaker (Fig. 8). The particles containing only Mn and Co (Fig. 8e, 8f) show  $00l$  reflections with approximately the same peak position and intensity distribution as those of Co,Ni particles, but they show only one hexagonal network of  $hk0$  reflections corresponding to sublattice I.

The SAED pattern of the cobalt asbolane was described by Chukhrov et al. (1982). In spite of an absence of Ni, the particles displayed patterns with two incommensurate hexagonal networks of  $hk0$  reflections that they attributed to two sublattices (I and II), with  $a_I = 2.84$  Å and  $a_{II} = 3.15$  Å. The 100, 110, and 200 reflection intensities belonging to sublattice I were the same as those for cobalt nickel asbolane particles [ $I(110) = 2I(100)$ ] whereas 100 and 110 reflections for sublattice II had approximately the same intensity.

Co and Mn RDF for the asbolane samples are plotted in Figure 9a. The strong second peak attests to the presence of a Me shell at 2.9 Å. The appearance of a weak third peak in the CoK RDF for sample asb was shown by analysis in the  $k$  space to result from a few corner-sharing (Co,Mn) octahedra. Such linkages are undetectable at the MnK edge by both EXAFS and pre-edge spectroscopy (Part I). One possible explanation for this effect is that the impurity in the cobalt busserite has a 2-D' struc-

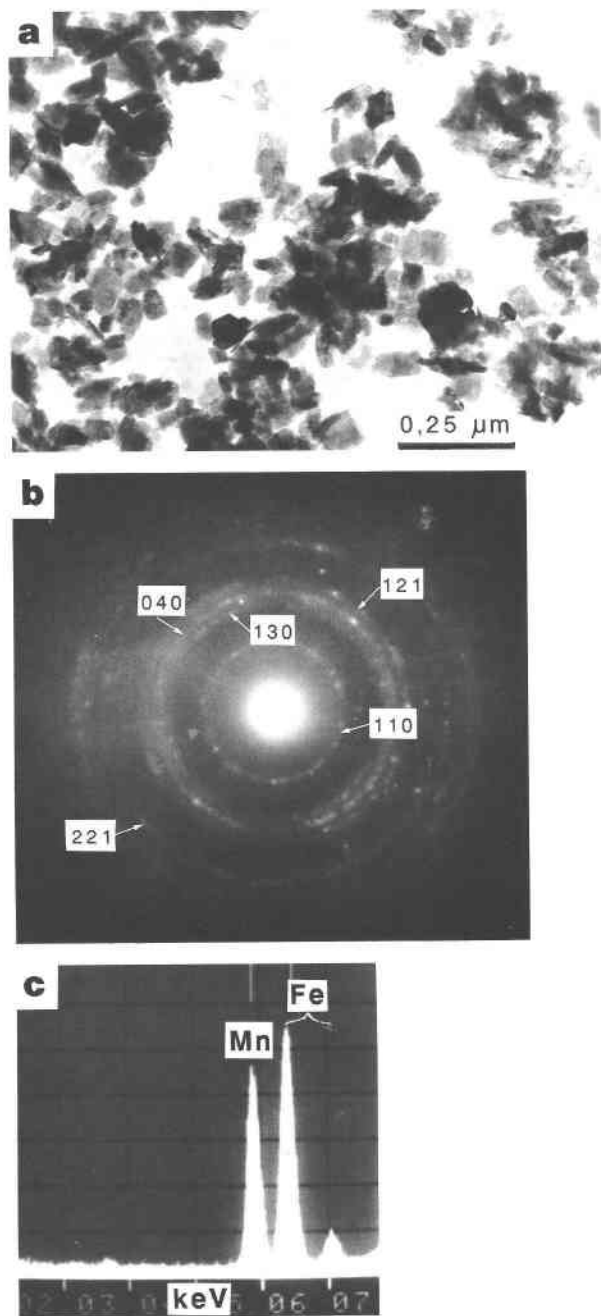


Fig. 6. (a) A TEM image of Mn-bearing goethite particles. (b) A SAED pattern of one of the particles; it resembles that of pure goethite. (c) A representative EDS spectrum.

ture. Analysis in the  $k$  space of the Co-O contributions for asbolane shows in phase backscattered waves (Fig. 9b). The coincidence of zero crossings proves that the Co distance is preserved from one sample to another. Manceau et al. (1987) reported 1.92 Å for this Co-O bond length. In order to test spectroscopic sensitivity to  $^{59}\text{Co}^{3+}$ , a simulated Co-O contribution at 1.77 Å has also been plotted in Figure 9b. This wave is out of phase in the high

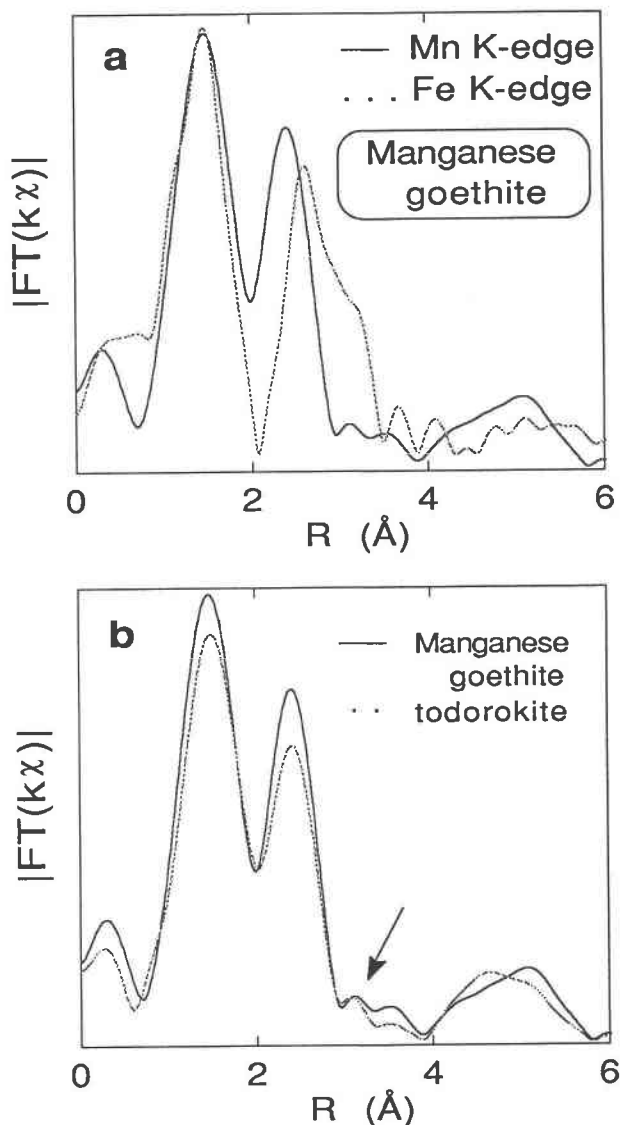


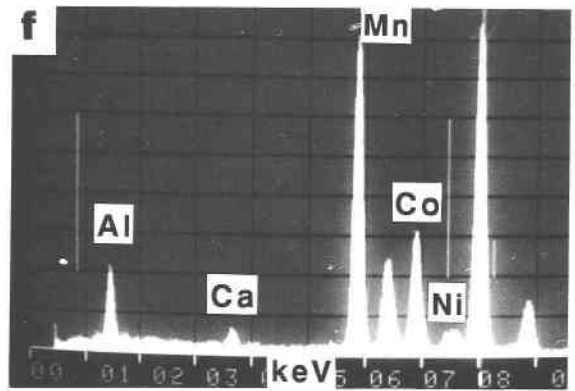
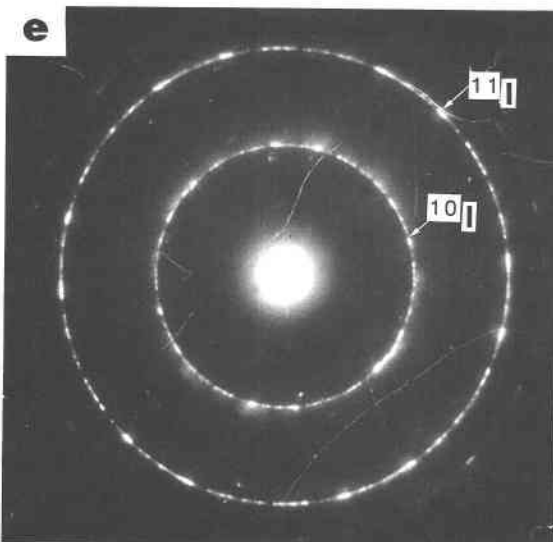
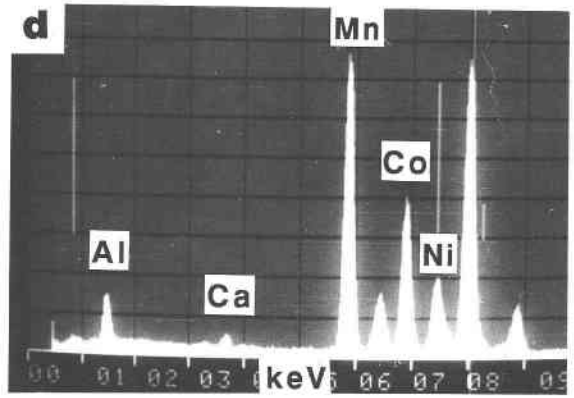
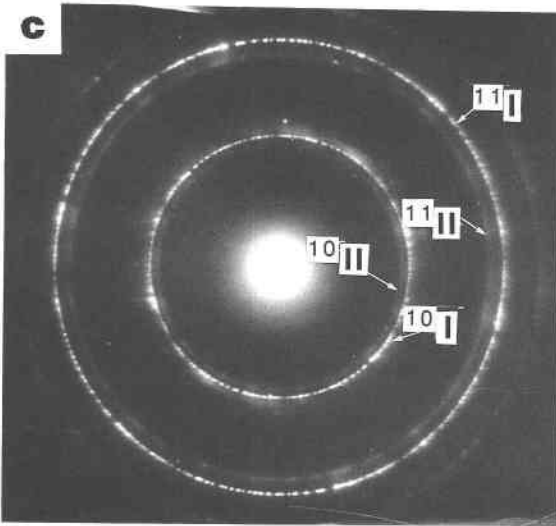
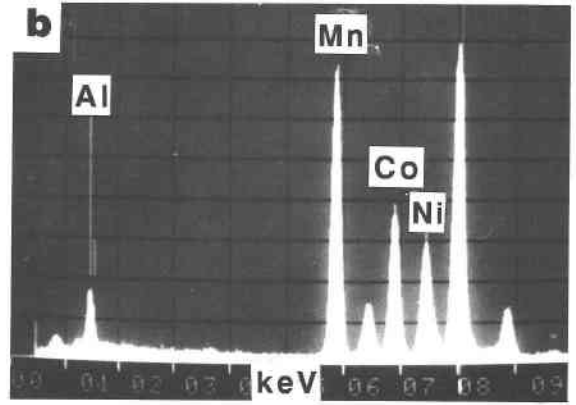
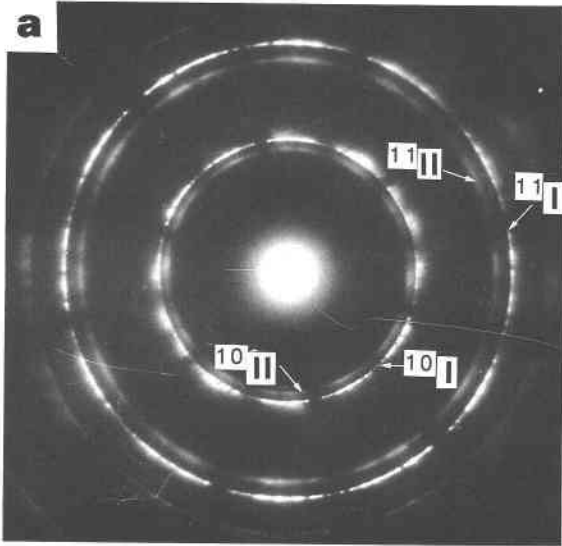
Fig. 7. EXAFS data for manganese goethite. (a) Comparison of Mn and FeK RDF. (b) Similarity of the MnK RDF of todorokite and manganese goethite. Notice their third peaks (arrow). RDF have not been corrected for phase shifts.

$k$  range ( $2k\Delta R \approx \pi$ ) rendering the overall wave envelope particularly sensitive to the presence of a small amount of  $^{59}\text{Co}^{3+}$ . A set of simulations shows that the detection limit of fourfold-coordinated Co is less than 15–20%. NiK EXAFS spectra of the two cobalt nickel asbolane samples are almost identical to that of  $\text{Ni}(\text{OH})_2$  (Manceau et al., 1987).

## DISCUSSION

### Birnessite

**Two-dimensional vs. 2-D' structure.** According to Giovanoli and coauthors (Giovanoli et al., 1969, 1970a, 1970b; Giovanoli and Stähli, 1970), synthetic sodium birnessite has a two-layer, orthorhombic unit cell. Its



structure was thought to be related to that of chalcophanite. Both structures have edge- and corner-sharing octahedra, but in the former, Mn was proposed to substitute for Zn in the interlayer region. With this 2-D' model, a third RDF peak typical of corner-sharing octahedra is expected. Because of Mn substitution for Zn, interlayer Mn atoms would absorb X-rays at the MnK edge, resulting in a stronger peak than that which occurs for chalcophanite (Fig. 1a). The detection limit of Mn neighbors being better than one atom at low temperature (Manceau and Combes, 1988), the absence of Mn<sup>4+</sup>-Mn<sup>4+</sup> pairings at 3.4–3.5 Å (Fig. 1b) indicates that no Mn<sup>4+</sup> ions occur at the Zn position. However, the presence of some low-valency Mn atoms (e.g., Mn<sup>2+</sup>) cannot be excluded from this study, as it would lead to larger Mn-Mn distances. The presence of Na, which has a small backscattering power, in the Zn position appears unlikely, since the adsorption of monovalent ions is usually nonspecific (Kiniburgh and Jackson, 1981), i.e., Na<sup>+</sup> is adsorbed at mineral surfaces by electrostatic attraction in the electrical double layer without establishing a chemical bond with the surface.

On the basis of the calculation of XRD patterns for different structural models, Chukhrov et al. (1985b) concluded that his birnessite sample (B1) had a 2-D' structure. However, with this method, it was impossible to determine the distribution of isomorphous Mn and Mg atoms among layer and interlayer octahedral sites. By comparison with the chalcophanite structure, Chukhrov et al. (1985b) proposed that interlayer sites above and below octahedral layer vacancies would more likely be filled with Mn than with Mg atoms. Now, in light of the preedge results (Part I) and the EXAFS results (no Mn corner sharing in sample B1), we suggest that Mn<sup>4+</sup> atoms are solely located within octahedral layers, whereas Mg atoms and possibly Mn<sup>2+</sup>/Mn<sup>3+</sup> occupy interlayer octahedral sites. Because divalent cations have higher specific adsorption capacity than monovalent cations, Mg and, to a lesser extent, Ca seem to be better candidates than Na<sup>+</sup> for filling octahedral sites above and below vacancies in MnO<sub>2</sub> layers.

The very small peak on the right side of the second RDF peak for sample M12 results from few Mn<sup>4+</sup>, Co, Ni, or Cu neighbors at 3.4–3.5 Å (Fig. 1b). The presence of Mn-Me corner-sharing octahedra at this distance can be accounted for by the absence of Na, Ca, and Mg cations and the presence of 3d elements. Thus, one may conclude that both natural and synthetic birnessite structures consist of octahedral layers containing Mn<sup>4+</sup>, but they have different layer stackings. These structures, then,

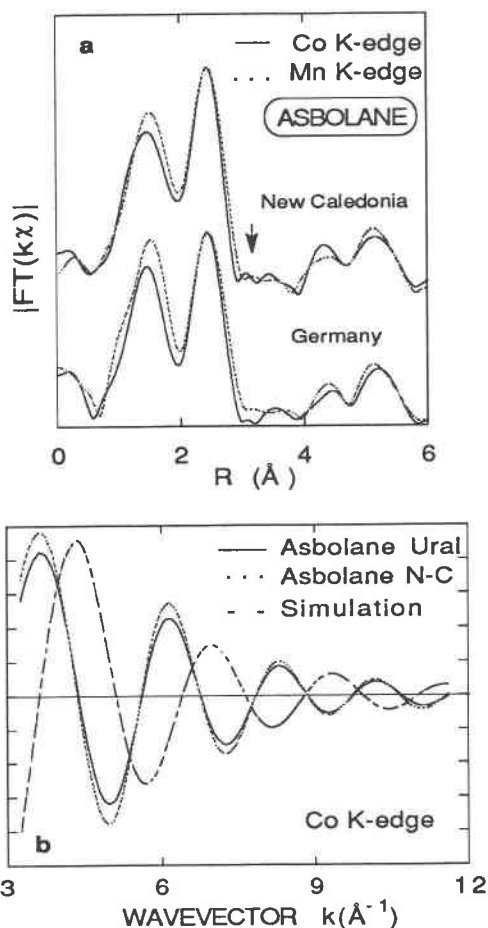


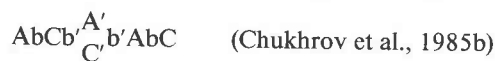
Fig. 9. EXAFS data for asbolane. (a) Comparison of normalized Mn and CoK RDF. Notice the presence of a small peak on the right side of the CoK RDF (arrow) indicating the presence of corner-sharing octahedra. (b) Comparison of Fourier-filtered Co(O,OH) contributions of New Caledonian and German asbolane and simulation assuming 4 O neighbors at 1.77 Å. Notice the phase shift.

may have Mn-Me corner-sharing octahedra that are detectable by EXAFS except when the metal site is filled with light cations like Mg or Ca. Where interlayer Na is present, strong corner sharing is unlikely.

**Layer stacking.** One of the interesting problems in determining the structural chemistry of birnessite is determination of the factors responsible for different layer stackings. One might suppose that the nature of exchangeable cations might have an effect. To test this hypothesis, let us consider birnessite structures in terms of

←  
Fig. 8. SAED patterns and EDS analyses for cobalt nickel asbolane particles (sample asb). For the particles having relatively high content of Ni, SAED patterns consist of two incommensurate  $hk$  reflection rings. The smaller the Ni content, the lower the intensity of the inner  $hk$  reflections. The SAED pattern for particles that contain only Mn and Co displays only one  $hk$  reflection ring. In all cases,  $I(10)_i \approx I(11)_i$ , where  $I(hk)$  is the intensity of the  $hk$  reflection, and  $i = I, II$  is for one of the two incommensurate  $hk$  reflection rings.

close-packed models. For natural one-layer hexagonal birnessite, the structure can be written symbolically as



where A and C represent the layer anion positions, A' and C', the H<sub>2</sub>O molecule sites, and b and b', the cations in octahedral sites within layers and interlayers, respectively. The location of divalent cations (Mg, Ca, Ni, or Cu) above and below vacant octahedral sites permits full local charge compensation because the charge of Mn<sup>4+</sup> ions is balanced by two divalent cations. In addition H<sub>2</sub>O molecules are arranged in the interlayer in such a way that, first, they form Mg octahedra with O located on one side of the interlayer (CA' and C'A stacking) and, second, they form empty prisms with O on the opposite side (A'A or CC' stacking). The H<sub>2</sub>O molecules and O atoms that form empty prisms in interlayers can then be connected by H bonds. Thus, the arrangement of divalent cations and H<sub>2</sub>O in natural birnessite compensates for local charge and enhances the cohesion of layers.

In synthetic birnessite, Na alone cannot provide local charge compensation. Therefore, the presence of Na in birnessite is expected to change the interlayer structure in such a way that favorable conditions are created for delocalized charge compensation and stabilization of layers. We will show that the sodium birnessite structure fulfills this expectation. By using the refinement achieved by the Rietveld method (Post and Veblen, 1990), the idealized one-layer monoclinic structure can be transformed into a three-layer rhombohedral close-packed model, resulting in the following sequence: AbCC'CaBB'BcAA'AbC . . . where A, B, C represent sites for layer O atoms; A', B', C' are sites for H<sub>2</sub>O molecules and Na cations of the interlayers; and a, b, c are layer octahedral sites. We see from the symbolic notation that H<sub>2</sub>O molecules form empty prisms with O atoms from two adjacent layers (AA'A, BB'B, and CC'C stackings). In the absence of local charge compensation, the arrangement of the interlayer species favors the formation of the H bonding between H<sub>2</sub>O molecules and O atoms. H bonding partly explains the difference between the observed structure and the idealized interlayer structure described above. It may also explain the distortion observed in the hexagonal symmetry of the layers (the value of  $a/\sqrt{3}$  in the monoclinic structure of sodium birnessite is much different than the value of the *b* parameter). Thus, H bonding is thought to be responsible for decreasing the space-group symmetry from 3R to C2/m or lower.

Our model suggests that the two-dimensional superperiodicity observed in SAED patterns from sodium birnessite in the past (Giovanoli et al., 1970a; Chukhrov et al., 1989; Post and Veblen, 1990) and in the present study results from a periodic distribution of Na atoms in the interlayer region, which is thought to result from electrostatic interaction. Under these conditions, the replacement of divalent cations by monovalent Na would lead to a new superperiodicity; i.e., the number of interlayer

cations would decrease, and electrostatic interactions between the remaining cations would increase. This predicted change of superperiodicity has actually been observed by Post and Veblen (1990).

The question is now the following: are there vacant sites in the layers of sodium birnessite? If there are no vacant sites, the two-dimensional superperiodicity would depend only on the degree of negative charge in the layer and on the valency of the exchangeable cations. If layers do contain vacant octahedral sites, divalent cations would be located above and below those vacancies irrespective of the layer charge. In the latter situation, superperiodicity displayed in SAED would reflect the actual distribution of vacant sites within layers. According to Post and Veblen (1990), exchange of Na for Mg promotes the reorganization of layer stacking and the arrangement of Mg ions and H<sub>2</sub>O molecules such that Mg ions nearly locate above and below layer octahedral sites. Such an arrangement of interlayer Mg is possible only if the underlying octahedral sites are empty. A second argument favoring the existence of layer octahedral vacancies comes from a description of the mechanism of Cr(III) oxidation to Cr(VI) by sodium birnessite. In Manceau and Charlet (1992) it is shown that aqueous free Cr<sup>3+</sup> ions diffuse to and fill in layer octahedral vacancies where the Cr<sup>3+</sup> to Mn<sup>4+</sup> electron transfer takes place.

### Vernadite

**Synthetic vernadite ( $\delta\text{-MnO}_2$ ).** Vernadite has a relatively large number of corner-sharing MnO<sub>6</sub> octahedra, as is shown by the shape of its RDF and by the XANES data (Part I). It is not yet clear whether the vernadite structure is closer to that of tectomanganate or phyllo-manganate of the 2-D' type. In the first hypothesis, vernadite would be built of multiple octahedral chains joined along their lengths by sharing vertices. In the second, it would have a layered structure with a few Mn atoms randomly removed from the layer plane to lie above or below vacant sites, as in the chalcophanite structure. In our opinion, vernadite should be regarded as a solid solution extending from phyllo-manganate to tectomanganate. It is more conveniently pictured as a 3-D (O,OH) framework, where cubic and hexagonal close-packing arrangements alternate at random and where octahedral sites are randomly filled, but where two adjacent Mn(O,OH)<sub>6</sub> octahedra cannot share faces. Such a model can be viewed as a mosaic of single and multiple octahedral chains of variable length ranging from 1 to *n* octahedra, and the chains are joined at corners. Because an equal average number of cations are located between every two adjacent anionic layers, neither XRD nor SAED patterns of  $\delta\text{-MnO}_2$  show basal reflections near 7, 3.5, or 2.35 Å. Thus,  $\delta\text{-MnO}_2$  cannot be regarded as a *c*-disordered birnessite as proposed by Giovanoli (1980a). Birnessite has either a 2-D or 2-D' structure, depending on the existence of octahedra that share corners, whereas  $\delta\text{-MnO}_2$ , like todorokite, has a 3-D anionic framework structure. As a result of birnessite's layered structure, its diffraction pattern should

contain basal reflections, even in the extreme case where the coherent scattering domains contain only a few layers, i.e., it is *c* disordered (Reynolds, 1980; Drits and Tchoubar, 1990). The XRD curve of an extremely disordered birnessite sample would then contain only two-dimensional *hk* bands and basal reflections whose positions would depend on the mean thickness of the coherent scattering domain (Drits and Tchoubar, 1990).

**Iron vernadite.** Simulation of the XRD pattern of hydrous oxides led Chukhrov et al. (1988) and Drits et al. (in preparation, a) to conclude that the absence of *hkl* reflections ( $l \neq 0$ ) is probably associated with (1) the mixing of cubic and hexagonal anionic packings, (2) the small size of coherent scattering domains, and (3) channels having different size and distribution patterns. The absence of basal reflections results from similar or identical cations within each pair of anionic layers. The observation by SAED of feroxyhite-like patterns simply indicates that hexagonal anionic packing prevails in Fe-rich particles. Data from XAS show that Fe and Mn atoms have different local structures and thus are segregated in domains. At the nanometer scale and on an average basis throughout the bulk, Fe octahedra belonging to Fe domains have the same interpolyhedral connections as in feroxyhite, i.e., face, edge, and corner sharing. Instead, Mn domains possess a 2-D' local structure. SAED and EDS results indicate that Mn- and Fe-containing domains are not space-separated phases, but they coexist within a unique coherent scattering domain.

Burns and Burns (1975, 1977) and Ostwald (1984) suggested that natural vernadite possesses a hybrid structure in which Mn and Fe atoms are segregated within irregularly intergrown monoatomic clusters. Mössbauer spectroscopy (Murad and Schwertmann, 1988) and EXAFS (Chukhrov et al., 1988; Manceau and Combes, 1988) demonstrated Fe and Mn segregation, but the intergrowth mechanism remains to be proved. EXAFS spectroscopy is unable to demonstrate whether epitaxial intergrowth occurs with either corner- or edge-sharing linkage or both, since it cannot distinguish Fe from Mn neighbors. However, chemical identity can be indirectly determined through the short-range order sensitivity of the preedge structure (cf. Part I). The low intensity of the preedges of ferruginous vernadite suggests a layerwise structure for Mn domains (Fig. 3c in Part I). In addition, third peaks are visible on MnK RDF (Fig. 3a), indicating corner sharing within Mn domains. These corner linkages are logically assigned to  $\text{MnO}_5\text{-O-Fe(O,OH)}$ , oxygen bridges.

### Mn-bearing goethite

Comparison of the Mn and Fe RDF for goethite demonstrates that Mn and Fe have different local structures; XANES (Part I) and EXAFS data show that Mn atoms are tetravalent. Thus the difference in oxidation state between Mn and Fe is the main deterrent to their random mixing among available octahedral sites. On the other hand, X-ray and electron diffraction data indicate that this mineral's structure is similar to that of homogeneous

goethite with a unique three-dimensional periodicity. With these limitations, determination of the structural location and distribution pattern of  $\text{Mn}^{4+}$  ions becomes a particularly interesting problem.

The mismatch in cell parameters between the isostructural minerals ramsdellite and goethite is less than 10% (Burns and Burns, 1975, 1977). One could then reasonably imagine an intimate intergrowth of these two phases. However, the Mn RDF of the manganese goethite sample more closely resembles those of todorokite and busserite than that of ramsdellite (Figs. 1a, 7b). This means that, unlike Fe, Mn octahedra mostly share edges with neighboring octahedra. Thus, we reject the hypothesis of a close ramsdellite-goethite association at the scale of the unit cell. The difference of the local environments of Mn and Fe, the relatively large number of edge linkages, and the weak preedge spectra that is characteristic of a 2-D structure (Fig. 3 in Part I) indicate that Mn atoms are segregated within a discrete phylломanganate-like local structure.

The question remains: do Mn clusters occur as a separate phase or do they have a definite structural relationship with the goethite lattice? A physical mixture of iron goethite and manganese phylломanganate within the sample would have been detected during electron and X-ray diffraction studies. The apparent discrepancy between information provided by EXAFS and the preedge spectroscopies (Part I) helps to determine how Mn clusters relate structurally to the rest of the mineral. EXAFS shows that  $\text{MnO}_6$  octahedra share as many corners as in todorokite (Fig. 7b), and from XANES we know that Mn clusters possess a roughly busserite-like local structure (Fig. 3 of Part I). This paradox is solved if one considers that the third MnK RDF peak is in part due to the existence of  $\text{MnO}_5\text{-O-Fe(O,OH)}$ , oxygen bridges. Although these results do not exclude the existence of edge linkages between Mn and Fe octahedra, one may postulate that some domains exist where octahedral Mn and Fe chains are joined only by corners. This local structure would resemble that already known in nsutite ( $\gamma\text{-MnO}_2$ ), where pyrolusite and ramsdellite domains are joined by corners.

Thus, the structural model for manganese goethite may be described as follows (Fig. 10a). The coherent scattering domains are determined by three-dimensional anionic frameworks that have a strong tendency to be hexagonally close-packed, resulting in *hkl* reflections in SAED and XRD patterns. Each coherent scattering domain includes Mn and Fe clusters linked through  $\text{MnO}_5\text{-O-Fe(O,OH)}$ , bridges. The cationic arrangement of Fe clusters is the same as for goethite, whereas Mn is distributed layerwise in Mn domains. The absence of basal reflections is accounted for by approximately the same number of cations between each O layer pair. The average structure can be defined in terms of a goethite-like cell because of the relatively regular distribution of filled and vacant octahedral sites. However, the vacant sites of the iron goethite unit cell must be replaced in the manganese goethite unit cell by some Mn, the quantity of which depends on the

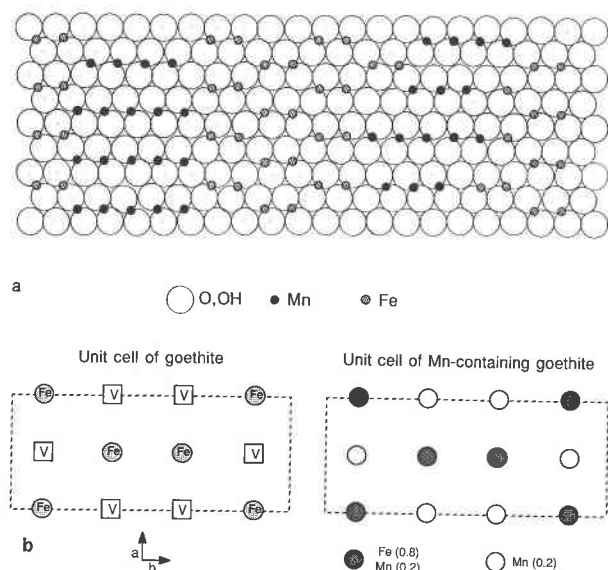


Fig. 10. A structural model for the Mn-bearing goethite. (a) Hexagonal anionic closed packing where domains of goethite and phyllomanganate are intergrown. (b) Distribution of cations over available octahedral sites in the unit cell of goethite and in the average unit cell of manganese goethite.

ratio between Fe and Mn atoms. Figure 10b shows a comparison of unit cells for pure goethite and a mineral containing 67 at% Fe and 33 at% Mn.

### Asbolane

The two incommensurate reciprocal sublattices described in the result section arise from the regular alternation of two layers. Their unit-cell parameters vary because of their different chemical compositions or structures. The ratio  $I(110)/I(100)$  has approximately the same value for reflections belonging to both sublattices, indicating that these layers have an identical structural motif. According to calculations made by Chukhrov et al. (1980), this intensity ratio is typical of octahedral layers.

We can combine data from all of the techniques (XANES, EXAFS, SAED, and EDS) to determine the structure of asbolane. From XANES, we learned that Co atoms are trivalent and sixfold coordinated, which agrees with a Co-(O,OH) distance of 1.92 Å (Manceau et al., 1987). This distance suggests a low-spin configuration, as high-spin  $^{60}\text{Co}^{3+}$  ions would result in a distance close to 1.99 Å (Chenavas et al., 1971). EXAFS data indicate that Mn and Co atoms possess an identical 2-D local structure, and it is impossible to use this method to determine whether Co substitutes for Mn in  $\text{MnO}_2$  layers or forms separate  $\text{CoOOH}$  layers. Nevertheless, in the SAED pattern of Ni-free particles from the cobalt nickel asbolane we see  $00l$  reflections with  $d(001) = 9.4$  Å. This indicates that two layers with different scattering powers alternate regularly and leads to the conclusion that one layer type corresponds to  $\text{MnO}_2$  and the other to  $\text{CoOOH}$  or

$\text{Co}(\text{OH})_3$ . The Co and Mn layers have the same size and are commensurate in the plane. Sublattice II corresponds to  $\text{Ni}(\text{OH})_2$  layer fragments that are free of both Co and Mn, explaining the progressive weakening of SAED reflections as Ni content decreases.

In cobalt asbolane, the appearance of two  $hk0$  reflection networks in combination with a unique series of  $00l$  reflections with  $d(001) = 9.4$  Å corresponds to two regularly alternating incommensurate layers. The distribution of  $hk0$  reflection intensities for sublattice II is quite different from that of cobalt nickel asbolane. Reflection intensity calculations led Chukhrov et al. (1982) to conclude that this mineral contains alternating tetrahedral and octahedral layers, but the similar scattering powers for Co and Mn prevent an unambiguous assignment of cations to particular sites. SAED, XANES, and EXAFS data make it clear that there are no tetrahedral  $\text{CoOOH}$  layers in cobalt asbolane. The  $a$  value of sublattice II ( $a_{II} = 3.15$  Å) is consistent with  $^{41}\text{Mn}^{2+}$  layers and cannot be attributed to any known  $^{60}\text{Co}^{3+}$  and  $^{61}\text{Mn}^{4+}$  layer structure. The presence of  $^{41}\text{Mn}^{2+}$  layers is then supported but not proved by our results. The relative concentration of  $\text{Mn}^{2+}$  in the bulk sample is below our XANES detection limit, and a lack of spatial resolution with EXAFS prevents observation of such a structure. Therefore, we propose a structure consisting of octahedral  $\text{MnO}_2$  layers alternating regularly with structural fragments of  $\text{Mn}(\text{OH})_2$ ; the position of Co atoms remains unknown.

### Atom segregation

One of the most interesting results of this study is the revelation of domain structure in natural hydrous oxides that contain some quantity of "foreign" cations. Domains having a different chemical composition or oxidation state of cations may have different structural relationships. The limiting case is represented by asbolane, where the domains are completely isolated. In cobalt nickel asbolane,  $\text{MnO}_2$ - $\text{Ni}(\text{OH})_2$  and possibly  $\text{CoOOH}$  layers coexist within the same crystal. Each layer is an independent structural fragment that alternates regularly in the  $c$  direction. Such a mixed-layer structure can be thought of as a polysome (Veblen, 1991), where slabs are sheet oxides of Mn and Ni. A second example is the pure manganese mixed-layer asbolane recently recognized by Butuzova et al. (1990). Here, Mn is presumably present in three incommensurate layers as  $\text{Mn}^{4+}$ ,  $\text{Mn}^{3+}$ , and  $\text{Mn}^{2+}$ . Likewise, the cobalt asbolane from Germany is thought to have alternating layers of  $\text{MnO}_2$  and  $\text{Mn}(\text{OH})_2$ .

The second class of domain structure is represented by iron vernadite and manganese goethite, where domains of different structure and cation composition are epitaxially inter- or overgrown within the same anion framework. In both minerals,  $\text{Mn}^{4+}$  ions have a strong tendency to combine by edge sharing of octahedra, but their main structural differences comprise the following: (1) the anion framework of manganese goethite is a hexagonal array, but in iron vernadite coherent scattering domains possess both hexagonal and cubic anionic packings; (2)

the Fe domains in the two minerals have a different cation distribution over available octahedral sites, resulting in a feroxyhite-like local structure in iron vernadite and a goethite-like local structure in manganese goethite.

### Structure of two-line hydrous oxides

Knowledge of the local structure of hydrous oxides is needed to understand the role of short-range cation ordering in the formation of long-range ordering. Indeed, in their highest disordered state, pure Mn and pure iron hydrous oxides usually display only two weak, broad *hk* bands (or "two lines") on X-ray and electron diffraction patterns. EXAFS data suggest at least five distinct local structures that can correspond to such a diffraction pattern; the actual local structure depends on how the gel formed. Ferric gels that are freshly precipitated after complete hydrolysis and oxidation of ferrous sulfate or chloride solutions at neutral pH show a lepidocrocite-like  $\gamma$ -FeOOH local structure (Combes et al., 1986). However, gels synthesized from a nitrate or chloride ferric solution show a goethite-like ( $\alpha$ -FeOOH) or akaganeite-like ( $\beta$ -FeOOH) local structure, respectively (Combes et al., 1989). When a goethite-like gel is heated (to 92 °C) for a few hours, it transforms into a feroxyhite-like, two-line gel, and subsequently into hematite (Combes et al., 1990). This last local structure has been observed in all of the natural two-line Fe gels studied up to now (the so-called protoferrihydrite; Combes, 1988). It is interesting that the interpolyhedral linkages that are typical of well-crystallized Fe minerals are already present in their pre-mineral gel. Thus, the structural formation of ferric oxyhydroxides ( $\alpha$ -,  $\beta$ -,  $\gamma$ -FeOOH) is undoubtedly decided very early in the polymerization process. On the other hand, the structure of two-line  $Mn^{4+}$  hydrous gels ( $\delta$ - $MnO_2$ ) seems not to be strictly related to that of the subsequent, well-crystallized polymorph. Mn gels most probably consist of a 3-D framework of randomly distributed edge- and corner-sharing  $MnO_2$  octahedra; that might explain why they seem able to transform into a large variety of structures.

It is evident from this discussion that diffraction effects from extremely disordered  $Mn^{4+}$  and  $Fe^{3+}$  hydrous oxides have low sensitivity to changes in local structures. The similarity of XRD patterns for all two-line compounds results from the fact that their coherent scattering domains have extremely small values (a few tens of thousands of cubic ångströms) and usually are composed of mixed cubic and hexagonal anionic packings, where each pair of anionic layers contains, on average, the same number of cations. Structural interpretations of these featureless diffraction patterns are hardly feasible and at least not always unique. The idea of adding about 33% tetrahedrally coordinated Mn and Fe to fit XRD profiles (Chukhrov et al., 1988; Eggleton and Fitzpatrick, 1988, 1990) is then to be treated with caution; the concept is not supported by Mössbauer spectroscopy (Cardile, 1988) and contradicts XANES and EXAFS results at both the Mn and FeK edges (Manceau et al., 1990b; Waychunas

et al., 1993; Part I). New structural models that satisfy both XRD and XAS results have been recently proposed for Fe hydrous oxides (Manceau and Drits, in preparation; Drits et al., in preparation, a, b) but remain to be established for Mn compounds.

### CONCLUSIONS

1. Natural magnesium birnessite has a one-layer hexagonal unit cell; synthetic sodium birnessite has a monoclinic subcell with structural similarity to chalcophanite but lacking corner-sharing  $Mn^{4+}$ - $Mn^{4+}$  octahedra. Structure of the interlayer and layer stacking are controlled by the nature of the interlayer cation. The structures of magnesium and sodium birnessite can be described using anionic close-packed layer models.

2. Synthetic vernadite ( $\delta$ - $MnO_2$ ) is not *c*-disordered birnessite. Its structure probably consists of a mosaic of single and multiple octahedral chains having variable length and width. The chains are joined by corners in a 3-D anionic framework. That there are the same mean number of cations in each two adjacent anionic layers explains the absence of *00l* reflections. The absence of *hkl* reflections results from structural disorder in the distribution of chain sizes, the small coherent scattering domains, and the mixture of anionic cubic and hexagonal packing.

3. The X-ray-amorphous hydrous iron manganese oxide phase called iron vernadite that occurs on the ocean floor has a hybrid structure with coexisting  $Mn^{4+}$  and  $Fe^{3+}$  domains. In one domain, Mn atoms are distributed layerwise, as in phyllo-manganate, whereas in the other, Fe octahedra are linked as in feroxyhite.

4. Natural manganese goethite, previously described as goethite-groutite, consists of  $Mn^{4+}$  and  $Fe^{3+}$  domains that have cation distributions similar to phyllo-manganate and goethite, respectively.

5. Cobalt nickel asbolane is formed by layers of  $MnO_2$ ,  $Ni(OH)_2$ , and possible  $CoOOH$  or  $Co(OH)_3$ , alternating regularly along the *c* axis. In cobalt asbolane,  $Mn^{2+}$  tetrahedral layers are probably regularly mixed with layers of  $MnO_2$ . However, additional experimental evidence for this structure is needed.

This study reemphasizes the complex structure of some low-temperature minerals. Structural variability and imperfection occur in the stacking of layered mineral structures such as birnessite. Much about their structure remains unknown, and one may foresee that birnessite with different degrees of periodicity in its two-dimensional layer stackings as well as with structural imperfections in the interlayer region will be found in natural environments. A second class of imperfection concerns the hybrid structure of low-temperature minerals at a very fine scale. Two types of structural situations have so far been identified: (1) a simple deviation from the random distribution of atoms in a solid solution series (Manceau, 1990), and (2) the existence of intimately mixed discrete phases. On one hand, these phases can entertain no structural relationship (except for the presence of H bonding) such as is

observed for asbolanes. On the other, they can be epitaxially intergrown, as is true for iron vernadite, manganese goethite, and iron diaspore (Hazemann et al., 1992). All these types of crystal defects result from nonequilibrium crystallization in the thermodynamic and kinetic conditions that prevail at the Earth's surface. For instance, epitaxial overgrowths are thought to result from a heterogeneous nucleation in conditions of undersaturation (Charlet and Manceau, 1992). Deciphering the actual structure of these and other complex minerals is an important first step toward an advance understanding of their conditions and mechanisms of formation.

### ACKNOWLEDGMENTS

The authors thank R. Giovanoli for providing the sodium birnessite sample and the staff of LURE for the synchrotron facility. A critical reading of a preliminary version by G.A. Waychunas is acknowledged. The authors express their gratitude to Susan Stipp, who helped improve the English. This research was supported by CNRS/INSU through the DBT program, grant 90 DBT 1.03 (contribution no. 414).

### REFERENCES CITED

- Blake, R.L., Hessevick, R.E., Zoltai, T., and Finger, L.W. (1966) Refinement of the hematite structure. *American Mineralogist*, 51, 123–129.
- Burns, R.G., and Burns, V.M. (1975) Mechanism for nucleation and growth of manganese nodules. *Nature*, 255, 130–131.
- (1977) Mineralogy of manganese nodules. In G.P. Glasby, Ed., *Marine manganese deposits*, p. 185–248. Elsevier, New York.
- Butuzova, G.Yu., Drits, V.A., Morozov, A.A., and Gorshkov, A.I. (1990) Processes of formation of iron manganese oxyhydroxides in the Atlantis II and Thetis Deep of the Red Sea. Special Publication of the International Association of Sedimentologists, 11, 57–72.
- Byström, A.M. (1949) The crystal structure of ramsdellite, an orthorhombic modification of  $MnO_2$ . *Acta Chemica Scandinavica*, 3, 163–173.
- Cardile, C.M. (1988) Tetrahedral  $Fe^{3+}$  in ferrihydrite:  $^{57}Fe$  Mössbauer spectroscopic evidence. *Clays and Clay Minerals*, 36, 537–539.
- Charlet, L., and Manceau, A. (1992) X-ray absorption spectroscopic study of the sorption of Cr(III) at the oxide/water interface. II. Adsorption, coprecipitation and surface precipitation on ferric hydroxides. *Journal of Colloid and Interface Science*, 148, 425–442.
- Chenavas, J., Joubert, J.C., and Marezio, M. (1971) Low-spin  $\rightarrow$  high-spin transition in high pressure cobalt sesquioxide. *Solid State Communications*, 9, 1057–1060.
- Chukhrov, F.V., Gorshkov, A.I., Sivtsov, A.V., and Berezovskaya, V.V. (1978a) Structural varieties of todorokite. *Izvestia Akademii Nauk, SSSR, Seriya Geologicheskaya*, 12, 86–95.
- Chukhrov, F.V., Gorshkov, A.I., and Rudnitskaya, E.S. (1978b) On vernadite. *Izvestia Akademii Nauk, SSSR, Seriya Geologicheskaya*, 6, 5–19.
- Chukhrov, F.V., Gorshkov, A.I., Sivtsov, A.V., and Berezovskaya, V.V. (1979) New data on natural todorokites. *Nature*, 278, 631–632.
- Chukhrov, F.V., Gorshkov, A.I., Vitovskaya, I.V., Drits, V.A., Sivtsov, A.V., and Rudnitskaya, Ye.S. (1980) Crystallochemical nature of Co-Ni asbolane. *International Geology Review*, 24, 5, 598–604 (translated from *Izvestia Akademii Nauk, SSSR, Seriya Geologicheskaya*, 6, 73–81).
- Chukhrov, F.V., Gorshkov, A.I., and Sivtsov, A.V. (1981) A new structural variety of todorokite. *Izvestia Akademii Nauk, SSSR, Seriya Geologicheskaya*, 5, 88–91.
- Chukhrov, F.V., Gorshkov, A.I., Drits, V.A., and Sivtsov, A.V. (1982) New structural varieties of asbolane. *Izvestia Akademii Nauk, SSSR, Seriya Geologicheskaya*, 6, 69–77.
- Chukhrov, F.V., Gorshkov, A.I., Drits, V.A., Shterenberg, L.Ye., Sivtsov, A.V., and Sakharov, B.A. (1983) Mixed-layer asbolane-buserite minerals and asbolanes in oceanic iron-manganese nodules. *International Geology Review*, 1983, 25, 838–847 (translated from *Izvestia Akademii Nauk, SSSR, Seriya Geologicheskaya*, 5, 91–99).
- Chukhrov, F.V., Gorshkov, A.I., Drits, V.A., and Dikov, Y.P. (1985a) Structural varieties of todorokite. *International Geology Review*, 1985, 27, 1481–1491 (translated from *Izvestia Akademii Nauk, SSSR, Seriya Geologicheskaya*, 11, 61–72).
- Chukhrov, F.V., Sakharov, B.A., Gorshkov, A.I., Drits, V.A., and Dikov, Y.P. (1985b) Crystal structure of birnessite from the Pacific Ocean. *International Geology Review*, 1985, 27, 1082–1088 (translated from *Izvestia Akademii Nauk, SSSR, Seriya Geologicheskaya*, 8, 66–73).
- Chukhrov, F.V., Gorshkov, A.I., and Drits, V.A. (1986) Crystallochemical systematics of Mn-minerals with tunnel structures. *Izvestia Akademii Nauk, SSSR, Seriya Geologicheskaya*, 10, 3–18.
- (1987a) News in crystallochemistry of manganese hydroxides. *Zapiski Vsesoyunogo Mineralogicheskaya Obchestva*, 116, 210–222.
- Chukhrov, F.V., Sakharov, B.A., Gorshkov, A.I., Drits, V.A., and Barinov, N.N. (1987b) New mixed-layer phase from oceanic Fe-Mn nodules. *Lithology and Row Materials*, 5, 112–120.
- Chukhrov, F.V., Drits, V.A., Gorshkov, A.I., Sakharov, B.A., and Dikov, Y.P. (1987c) Structural models of vernadites. *Izvestia Akademii Nauk, SSSR, Seriya Geologicheskaya*, 12, 198–204.
- Chukhrov, F.V., Manceau, A., Sakharov, B.A., Combes, J.-M., Gorshkov, A.I., Salyn, A.L., and Drits, V.A. (1988) Crystal chemistry of oceanic Fe-vernadites. *Mineralogicheskii Zhurnal*, 10, 78–92.
- Chukhrov, F.V., Gorshkov, A.I., and Drits, V.A. (1989) Supergenic manganese hydroxides, 208 p. Nauk, Moscow.
- Combes, J.-M. (1988) Evolution de la structure locale des polymères et gels ferriques lors de la cristallisation des oxydes de fer. Application au piégeage de l'uranium. Thèse de Doctorat, Université Paris 6, Paris.
- Combes, J.-M., Manceau, A., and Calas, G. (1986) Study of the local structure in poorly-ordered precursors of iron oxy-hydroxides. *Journal de Physique*, C8, 697–701.
- Combes, J.-M., Manceau, A., Calas, G., and Bottero, J.-Y. (1989) Formation of ferric oxides from aqueous solutions: A polyhedral approach by X-ray absorption spectroscopy. I. Hydrolysis and formation of ferric gels. *Geochimica et Cosmochimica Acta*, 53, 583–594.
- Combes, J.-M., Manceau, A., and Calas, G. (1990) Formation of ferric oxides from aqueous solutions: A polyhedral approach by X-ray absorption spectroscopy. II. Hematite formation from ferric gels. *Geochimica et Cosmochimica Acta*, 54, 1083–1091.
- Delaplane, R.G., Ibers, J., Ferraro, J.R., and Rush, J.J. (1969) Diffraction and spectroscopic studies of the cobaltic acid system  $HCoO_2 \cdot DCoO_2$ . *Journal of Chemical Physics*, 50, 1920–1927.
- Deliens, M., and Goethals, H. (1973) Polytypism of heterogenite. *Mineralogical Magazine*, 39, 152–157.
- Drits, V.A. (1987) Electron diffraction and high-resolution electron microscopy of mineral structures. Springer-Verlag, Berlin.
- Drits, V.A., and Tchoubar, C. (1990) X-ray diffraction of disordered lamellar structures. Theory and application to microdivided silicates and carbons. Springer-Verlag, Berlin.
- Drits, V.A., Petrova, V.V., and Gorshkov, A.I. (1985) Manganese minerals of Fe-Mn nodules from the sediments of the central part of Pacific Ocean and their postsedimentation transformation. *Lithology and Raw Materials*, 3, 17–39.
- Eggleton, R.A., and Fitzpatrick, R.W. (1988) New data and a revised structural model for ferrihydrite. *Clays and Clay Minerals*, 36, 111–124.
- (1990) New data and a revised structural model for ferrihydrite: Reply. *Clays and Clay Minerals*, 38, 335–336.
- Ewing, F.J. (1935) The crystal structure of lepidocrocite,  $\gamma\text{-FeOOH}$ . *Journal of Chemical Physics*, 3, 420–427.
- Giovanoli, R. (1980a) Vernadite is random-stacked birnessite. *Mineralium Deposita*, 15, 251–253.
- (1980b) On natural and synthetic manganese nodules. In I.M. Valentsov and G. Grassley, Eds., *Geology and geochemistry of manganese*, vol. 1, p. 159–202. Schweizerbart'sche Verlagsbuchhandlung, Stuttgart.
- Giovanoli, R., and Stähli, E. (1970) Oxide und Oxidhydroxide des drei- und vierwertigen Mangans. *Chimia*, 24, 49–61.
- Giovanoli, R., Stähli, E., and Feitknecht, W. (1969) Über Struktur und Reaktivität von Mangan (IV) Oxiden. *Chimia*, 23, 264–266.

- (1970a) Über Oxyhydroxide des vierwertigen Mangans mit Schichtengitter. 1. Natrium Mangan (II,III)-Manganat (IV). *Helvetica Chimica Acta*, 53, 209–220.
- (1970b) Über Oxidhydroxide des vierwertigen Mangans mit Schichtengitter. 2. Mangan (III)-Manganat (IV). *Helvetica Chimica Acta*, 53, 453–464.
- Hazemann, J.L., Manceau, A., Sainctavit, P., and Malgrange, C. (1992) Structure of the  $\alpha\text{Fe}_2\text{Al}_{1-x}\text{OOH}$  solid solution. Evidence by polarized EXAFS for an epitaxial growth of hematite-like clusters in diaspore. *Physics and Chemistry of Minerals*, 19, 25–38.
- Kinniburgh, D.G., and Jackson, M.L. (1981) Cation adsorption by hydrous metal oxides and clay. In M.A. Anderson and A.J. Rubin, Eds., *Adsorption of inorganics at solid-liquid interfaces*, p. 91–160. Ann Arbor Science, Ann Arbor, Michigan.
- Manceau, A. (1989) Synthetic 10-Å and 7-Å phyllosulfates: Their structures as determined by EXAFS—Discussion. *American Mineralogist*, 74, 1386–1389.
- (1990) Distribution of cations among the octahedra of phyllosulfates: Insight from EXAFS. *Canadian Mineralogist*, 28, 321–328.
- Manceau, A., and Charlet, L. (1992) X-ray absorption spectroscopic study of the sorption of Cr(III) at the oxide/water interface. I. Molecular mechanism of Cr(III) oxidation on Mn oxides. *Journal of Colloid and Interface Science*, 148, 443–458.
- Manceau, A., and Combes, J.-M. (1988) Structure of Mn and Fe oxides and oxyhydroxides: A topological approach by EXAFS. *Physics and Chemistry of Minerals*, 15 (3), 283–295.
- Manceau, A., Llorca, S., and Calas, G. (1987) Crystal chemistry of cobalt and nickel in lithiophorite and asbolane from New Caledonia. *Geochimica et Cosmochimica Acta*, 51, 105–113.
- Manceau, A., Combes, J.-M., and Calas, G. (1989) Chemical and structural applications of X-ray absorption spectroscopy in mineralogy. *Journal de Chimie Physique*, 86, 1533–1546.
- Manceau, A., Buseck, P.R., Miser, D., Rask, J., and Nahon, D. (1990a) Copper site occupancy in lithiophorite from a Mn banded ore. *American Mineralogist*, 75, 490–494.
- Manceau, A., Combes, J.-M., and Calas, G. (1990b) New data and a revised model for ferrihydrite: A comment on a paper by R.A. Eggleton and R.W. Fitzpatrick. *Clays and Clay Minerals*, 38, 331–334.
- Manceau, A., Gorshkov, A.I., Drits, V.A. (1992) Structural chemistry of Mn, Fe, Co, and Ni in manganese hydrous oxides: Part I. Information from XANES spectroscopy. *American Mineralogist*, 77, 1133–1143.
- Miura, H. (1986) The crystal structure of hollandite. *Mineralogical Journal*, 13, 119–129.
- Murad, E., and Schwertmann, U. (1988) Iron oxide mineralogy of some deep-sea ferromanganese crusts. *American Mineralogist*, 73, 1395–1400.
- Ostwald, J. (1984) Ferruginous vernadite in an Indian Ocean ferromanganese nodule. *Geological Magazine*, 121, 483–488.
- Patrat, G., De Bergevin, F., Perret, M., and Joubert, J.C. (1983) Structure locale de  $\delta\text{FeOOH}$ . *Acta Crystallographica*, B39, 165–170.
- Post, J.E., and Appleman, D.E. (1988) Chalcophanite,  $\text{ZnMn}_3\text{O}_7 \cdot 3\text{H}_2\text{O}$ : New crystal-structure determination. *American Mineralogist*, 73, 1401–1404.
- Post, J.E., and Bish, D.L. (1988) Rietveld refinement of the todorokite structure. *American Mineralogist*, 73, 861–869.
- Post, J.E., and Veblen, D.R. (1990) Crystal structure determinations of synthetic sodium, magnesium, and potassium birnessite using TEM and the Rietveld method. *American Mineralogist*, 75, 477–489.
- Post, J.E., Dreele, R.B., and Buseck, P.R. (1982) Symmetry and cation displacements in hollandites: Structure refinements of hollandite, cryptomelane and priderite. *Acta Crystallographica*, B38, 1056–1065.
- Potter, R.M., and Rossman, G.R. (1979) The tetravalent manganese oxides: Identification, hydration, and structural relationships by infrared spectroscopy. *American Mineralogist*, 64, 1199–1218.
- Reynolds, R.C. (1980) Interstratified clay minerals. In G.W. Brindley and G. Brown, Eds., *Crystal structures of clay minerals and their X-ray identification*, 495 p. Mineralogical Society, London.
- Sainctavit, P., Petiau, J., Manceau, A., Rivallant, R., Belakhovsky, M., and Renaud, G. (1988) A two-mirror device for higher harmonic rejection. *Nuclear Instruments Methods*, 273, 423–428.
- Stouff, P., and Boulègue, J. (1988) Synthetic 10 Å and 7 Å phyllosulfates: Their structures as determined by EXAFS. *American Mineralogist*, 73, 1162–1169.
- Strobel, P., Charenton, J.C., and Lenglet, M. (1987) Structural chemistry of phyllosulfates: Experimental evidence and structural models. *Revue de Chimie Minérale*, 24, 199–220.
- Szytula, A., Burewicz, A., Dimitrijevic, Z., Krasnicki, S., Rzany, H., Todorovic, J., Wanic, A., and Wolski, W. (1968) Neutron diffraction studies of  $\alpha\text{-FeOOH}$ . *Physica Status Solidi*, 26, 429–434.
- Szytula, A., Balanda, M., and Dimitrijevic, Z. (1970) Neutron diffraction studies of  $\beta\text{-FeOOH}$ . *Physica Status Solidi*, 3, 1033–1037.
- Teo, B.K. (1986) EXAFS: Basic principles and data analysis, 349 p. Springer-Verlag, Berlin.
- Towe, K.M., and Bradley, W.F. (1967) Mineralogical constitution of colloidal “hydrous ferric oxides.” *Journal of Colloid and Interface Science*, 24, 384–392.
- Turner, S., and Buseck, P.R. (1981) Todorokites: A new family of naturally occurring manganese oxides. *Science*, 212, 1024–1027.
- Veblen, D.R. (1991) Polysomatism and polysomatic series: A review and applications. *American Mineralogist*, 76, 801–826.
- Vicat, J., Franchon, E., Strobel, P., and Tran Qui, D. (1986) The structure of  $\text{K}_{1-3}\text{Mn}_8\text{O}_{16}$  and cation ordering in hollandite-type structures. *Acta Crystallographica*, B42, 162–167.
- Wadsley, A.D. (1953) The crystal structure of psilomelane,  $(\text{Ba}, \text{H}_2\text{O})_2\text{Mn}_3\text{O}_{10}$ . *Acta Crystallographica*, 6, 433–438.
- Waychunas, G.A., Rea, B.A., Fuller, C.C., and Davis, J.A. (1993) Surface chemistry of ferrihydrite. I. EXAFS studies of the geometry of coprecipitated and adsorbed arsenate. *Geochimica et Cosmochimica Acta*, in press.

MANUSCRIPT RECEIVED AUGUST 15, 1990

MANUSCRIPT ACCEPTED JULY 6, 1992